
Article:
Mapplebeck, S orcid.org/0000-0002-8223-186X, Booth, J and Shalashilin, D orcid.org/0000-0001-6104-1277 (2021) Simulation of protein pulling dynamics on second time scale with boxed molecular dynamics. The Journal of Chemical Physics, 155 (8). 085101. ISSN 0021-9606

https://doi.org/10.1063/5.0059321

Simulation of protein pulling dynamics on second timescale with Boxed Molecular Dynamics.

Sarah Mapplebeck, Jonathan Booth[1] and Dmitrii Shalashilin[2]

School of Chemistry, University of Leeds, Leeds LS2 9JT, U.K

ABSTRACT

We demonstrate how recently developed Boxed Molecular Dynamics (BXD) and kinetics [1] can provide a kinetic description of protein pulling experiments, allowing a connection to be made between experiment and atomistic protein structure. BXD theory applied to Atomic Force Microscopy unfolding is similar in spirit to the kinetic two state model [2] but with some differences. First, BXD uses large number of boxes and therefore it is not a two-state model. Second, BXD rate coefficients are obtained from atomistic Molecular Dynamics (MD) simulations. BXD can describe the dependence of the pulling force on pulling speed. Similarly to the ref [1] we show BXD is able to model the experiment on very long timescale up to seconds, which is way out of reach for standard molecular dynamics.

1. INTRODUCTION

Proteins are important biological molecules which play a crucial role in many of the body's functions. Titin for example, is a molecular spring responsible for the elastic response of sarcomeres within skeletal muscle, allowing it to stretch and recoil aiding movement.[3,4] As it is continually subject to mechanical forces, flexibility and mechanical robustness are critical attributes for the effective function of titin.[5]

The mechanical properties of proteins have been probed by Atomic Force Microscopy (AFM), a type of force spectroscopy in which protein domains are unfolded by pulling them either at a constant velocity or with a constant force. In this work we will focus on the constant velocity pulling experiments (CV AFM). [6,7]

[1] Current address: Croda Europe Ltd. Cowick Hall, Snaith, Goole, East Yorkshire, DN14 9AA, UK

[2] Corresponding author, e-mail: D.Shalashilin@leeds.ac.uk

In these experiments one end of the protein is adsorbed from solution onto a flat surface, before bringing in the cantilever to bind with the other.[6,8,9] Once bound, the cantilever is pulled away from the surface and the protein domains stretch and unfold. The deflection of the cantilever from its original position is then measured and multiplied by the spring constant of the cantilever to get the force as a function of extension.[5]

This produces the characteristic sawtooth pattern of a growing force with extension followed by a rapid decrease to almost zero. Analysis of such profiles suggests the rising phase of the sawtooth reflects the elasticity of the protein and the linker molecule attaching it to the AFM cantilever as they are stretched. [9,10] Figure 1 sketches a typical outcome of a single domain unfolding experiment and its interpretation. The domains are connected in sequence. At point 1 the element B of the concatemer is ruptured and the cantilever is relaxed. Then B is extended up to the point 2 when it is almost straight and stress is now put on the next unfolding element E, shown in red. At point 3 the stress reaches its maximum and E is ruptured. This coincides with a rapid reduction of the force as the cantilever 'snaps back' and the almost vertical edge of the sawtooth is produced between points 3 and 4. The cantilever relaxes to its equilibrium at point 4 and the element E unfolds further without resistance and the cycle repeats for the next unfolding element (A, C, D or F).

The extension of the domain between points 1 and 3 often shows smaller unfolding events, when weaker structures within protein domains are ruptured. One of such events is indicated as 3' at the figure 1. Thus, the region 1-3'-2 of the tooth shown in figure 1 can correspond further extension of domain B, followed by the rupture of domain E in the region 2-3-4. Or alternatively peak 3' can correspond to an intermediate unfolding event, such as the partial break of E before its strongest bonds are broken in the main rupture event. The peak forces, i.e. the forces at the points 3 or 3' are of particular interest as they determine the mechanical properties of the protein molecule.

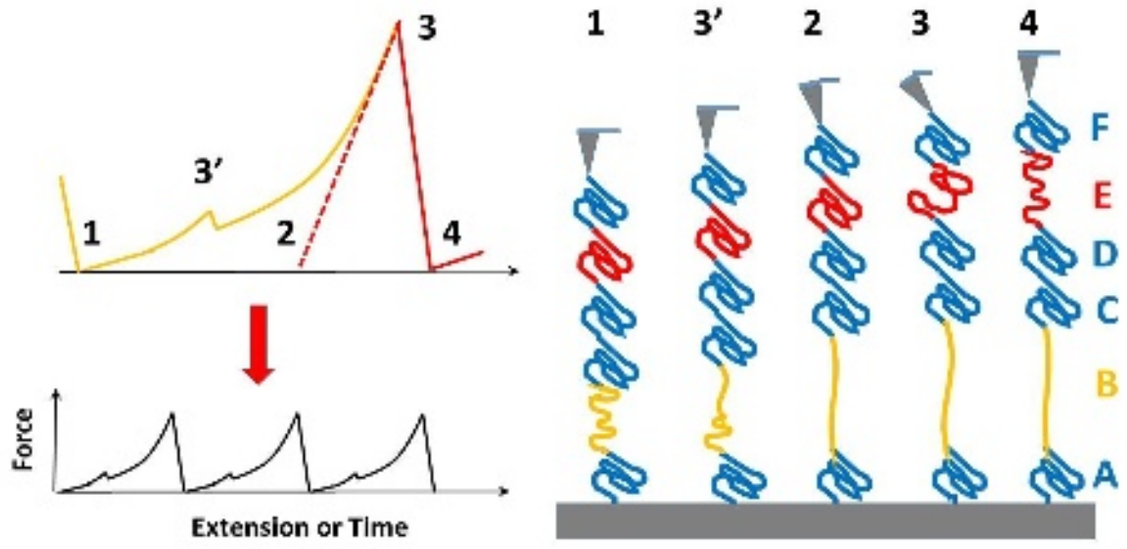

Figure 1. In an AFM pulling experiment the point 1 corresponds to concatemer element B (orange) being ruptured but not fully extended. At this point the cantilever is at equilibrium. Then the element B is extended, and the cantilever deforms producing Hooke's force. At point 2 B is nearly fully extended and the next unfolding element E (red) comes under stress. At point 3 the stress reaches its maximum and E raptures. Then between the points 3 and 4 the cantilever "snaps back" and E "gives away its slack". After that the cycle repeats for one of the remaining unfolded domains. On the tooth shaped image, the unfolding events of the domains B and E are indicated by corresponding colors. The extension of a domain can reveal smaller unfolding events, one of which is indicated as 3'. The unfolding forces F_{unfld} which rupture the protein structures are the forces at points 3 and 3'.

Recently, interesting phenomena in constant speed unfolding experiments have been observed which can potentially shed some light not only on the structure of the protein but also on the kinetics of the unfolding. These experiments have shown that rupture force, i.e. the force at the point 3 (or 3') at the figure 1, may depend on pulling velocity[8,9,11]. It was demonstrated that when pulling at intermediate velocities speed (<100 μm/s) the unfolding force often varies linearly with the log of pulling velocity.[9,12]

Theoretical explanation of this phenomenon is usually based on the two-state model which assumes the presence of, first, the folded state with the protein in its native structure and the pulling cantilever spring stretched, and second, the unfolded state with the protein ruptured and the cantilever spring at equilibrium. In the absence of pulling the unfolding rate given by transition state theory (TST) would be $k_u^o = \kappa v e^{\frac{-\Delta G_{TS-N}}{k_B T}}$ where κ is the phenomenological

transmission coefficient, ν is the vibrational frequency at the TS, $\Delta G_{\text{TS-N}}$ is the activation energy for unfolding, k_B is the Boltzmann constant and T is the temperature. When additional force is applied to pull the protein by the cantilever spring, the additional term W, the work of pulling force, should be added to the TS free energy. This decreases the free energy, so that the impact of mechanical force on unfolding includes an additional factor and now $k_u = \kappa\nu e^{\frac{-(\Delta G_{TS-N} - W)}{k_B T}} = k_u^0 e^{\frac{W}{k_B T}}$. This so-called Bell-Evans model assumes that the force is constant during the whole process of unfolding so that $W = -Fx$ where x is extension of the protein. Bell's model successfully explains the experimentally observed logarithmic dependence. [13]

A more sophisticated model [2] takes into account the effect of the pulling more accurately assuming that the pulling cantilever is a harmonic spring so that the work of pulling force includes a quadratic term, with respect to the extension of the protein. This model predicts that at very slow pulling speeds the pulling force is independent of the speed, which is followed by Bell-Evans logarithmic dependence at higher speeds.[9,11,14]

Constant speed experiments have been considered in the refs [8,15] where another microscopic model has been suggested, which addresses the differences in the dynamics of unfolding at low and high pulling velocities. First, when approaching the limit of slow pulling velocities, the cantilever works to hold back the molecular coordinate, resulting in slower rupture and a negative average unfolding force.[15,16] Secondly, at intermediate velocities often used in AFM experiments ($\nu = 10^{-1}$ - 10 μm/s) both pulling and stochastic motion contribute to the unfolding force which averages to an approximate linear dependency on the logarithm of pulling velocity similar to that predicted by phenomenological models. [9,13,15,17] The third region described by this model occurs at extremely high pulling speeds (> 100 μm/s) at which point stochastic motion becomes irrelevant and the dynamics becomes deterministic as there is insufficient time for proper exploration of the energy landscape. Here, TST breaks down as a steady influx into

the TS cannot be maintained, and so Bell's model which Dembo *et. al.* suggest is only valid for diffusive barrier crossings at small forces is no longer valid.[18]

Recently, it has been demonstrated experimentally that high-speed AFM (>100 μm/s) may result in a more complicated dependence of the force vs speed. An increase of the force above that of linear Bell-Evans force vs logarithm of pulling speed dependence has been observed. [8]

In principle, it should be possible to compare experiment with MD simulations. However, AFM experiments usually take place on micro to millisecond timescale,[19,20] or even longer, which is out of reach of standard unbiased MD simulations. In straightforward MD simulations, the velocity and force with which the protein is pulled is increased to much higher levels than in experiment.[21,22] A number of Steered Molecular Dynamics (SMD) simulations, which involve extending the end-to-end distance of protein domains by pulling with a virtual harmonic spring at a constant velocity[23] have been performed. The velocity used in MD simulations is much faster than experiment, by as much as six orders of magnitude. Therefore, direct comparison of experimental and simulated results is still unachievable with this method.[12]

Only recently it was possible to perform AFM at sufficiently high pulling speeds and conduct steered molecular dynamics simulations over long enough timescales for the uppermost and lowermost velocities of the respective methods to overlap.[8] However, the majority of the experimental speeds are still way out of reach of atomistic MD and can be described by phenomenological models only.

In the recent years we have been developing BXD, a method to speed up atomistic simulations and enable us to look at processes occurring over very long timescales.[1,24–27] BXD involves partitioning the phase space of a system into boxes by placing a series of reflective boundaries along the reaction coordinate. Rate constants for diffusion of a trajectory across these boundaries can be calculated in each direction by short time MD simulations, and from

these so too can the free energy along the reaction coordinate.[25,27] If a reaction coordinate is available BXD allows the dynamics to be described efficiently along such coordinate. In the past we were able to capture nontrivial nonstatistical effects with BXD, which cannot be described by TST.[1] In this paper we attempt to use BXD to simulate protein unfolding. Unlike the MD methods, the low and the moderate velocities seen in experimental AFM are accessible to BXD.[1,24–27]

The first advantage of BXD in comparison with the two-state model is that BXD can account for complicated kinetic effects and describe kinetics far from equilibrium (if any). The second advantage is that BXD kinetic coefficients are not phenomenological parameters like in the theory.[2,15]. They are obtained from fully atomistic MD and BXD does not make any assumptions except those already made about the MD force field.

In this paper we show how the dynamics of AFM unfolding can be modelled based on the results of our previous work [[24]]. BXD allows us to see the dynamics of unfolding and to obtain the force as a function of time and cantilever position, the quantities measured in the experiment. The timescales of slow pulling are way out of reach of normal MD simulations. According to our BXD simulations the unfolding force should be affected by the stiffness of the cantilever. Such dependence should allow additional information about the thermodynamics of the unfolding Transition State to be extracted. To our best knowledge no systematic investigation of cantilever force constant influence on the outcome of pulling experiments have been performed and we propose such experiment.

2. THEORY

2.1 Boxed Molecular Dynamics

BXD is a simple technique which extends the timescales accessible to atomistic MD simulations and has therefore found use in the simulation of rare events such as protein folding

and cyclisation.[1,24–27] Figure 2 shows BXD in its most simple form, in which it is assumed that an atomistic process can be described by a reduced description of the configuration space of the system – a reaction coordinate or order parameter which can be split into multiple boxes into which the dynamics of a trajectory can be locked.

Each time a trajectory in box m collides with the boundary separating box m from its subsequent box, its velocity along the reaction coordinate is reversed as if it had collided with a hard wall. Counting the average number of boundary collisions or "hits" per unit of time is used to give the rate coefficients for the diffusion of the trajectory into one of its neighboring boxes, m+1 or m-1. This is done by dividing the number of "hits" against a particular boundary, $h_{m,m+1}$ or $h_{m+1,m}$ by the lifetime of the trajectory within the box t_m.

$$k_{m,m+1} = \frac{h_{m,m+1}}{t_m}$$
$$k_{m,m-1} = \frac{h_{m,m-1}}{t_m} \quad (1)$$

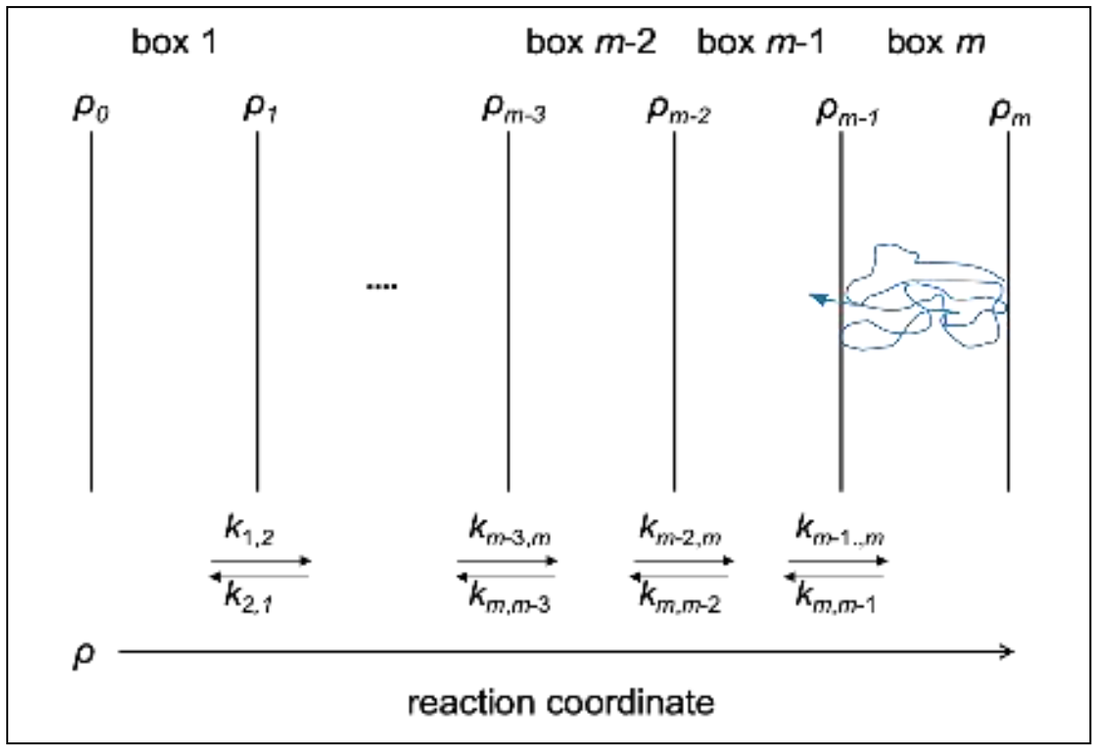

Figure 2. Schematic of BXD, where a reaction coordinate, ρ, is split into m boxes into which a trajectory can be confined. After a given number of inversions (2 in this case) the trajectory in box m can diffuse across the boundary into box m-1. Dividing the number of hits at boundary $h_{m,m-1}$ by the lifetime of the trajectory in the box gives a rate coefficient for diffusion into box m-1. This process is repeated until the trajectory has sampled up and down entire reaction coordinate multiple times generating a set of box-to-box rate coefficients.

Once sufficient statistics have been collected, the trajectory is allowed to move into the next box and the process is repeated. In practice, the trajectory is allowed to sample all boxes along the entire reaction coordinate multiple times in both forward and backwards directions until convergence of rate coefficients is achieved. Eventually, rate coefficients for exchange between neighboring boxes are accumulated, and the dynamics is reduced to a set of kinetic equations

$$\begin{aligned}
\frac{dn_1(t)}{dt} &= -k_{12}(t)n_1(t) + k_{21}n_2(t) \\
\frac{dn_2(t)}{dt} &= k_{12}(t)n_1(t) + k_{32}(t)n_3(t) - \big(k_{21}(t) + k_{23}(t)\big)n_2(t) \\
&\cdots \\
\frac{dn_m(t)}{dt} &= k_{m-1,m}(t)n_{m-1}(t) - k_{m,m-1}(t)n_m(t)
\end{aligned} \tag{2}$$

where n is the population of the subscripted box as a function of time, described by the flux into minus the flux out of each box. Equation 2 can be written in the matrix form

$$\frac{\mathrm{d}\mathbf{n}(\mathrm{t})}{\mathrm{dt}} = \mathbf{M}\mathbf{n}(\mathrm{t}) \tag{3}$$

where **n** is the vector of box populations, and the elements of the sparse matrix **M** are expressed via the rate coefficients in eq 1. Then the long-time MD simulation of the system is replaced by the solution of eq 3, the kinetic master equation (KME)

$$\mathbf{n}(\mathrm{t}) = \mathbf{U}\boldsymbol{\Lambda}\mathbf{U}^{-1}\mathbf{n}(0) \tag{4}$$

where **n**(0) contains the initial conditions for box populations, **U** is the eigenvector matrix resulting from diagonalisation of **M**, and **Λ** is a diagonal matrix whose elements, $\Lambda_{ij} = e^{\lambda jt}$, are determined by λ, the eigenvalue vector corresponding to **M**.

Thus, BXD replaces long time MD with a set of short time simulations localised in all boxes along the reaction coordinate. BXD with two boxes was proposed in the ref [28]. BXD is also related to the Intramolecular Dynamics Diffusion Theory (IDDT) where the idea of recovering long time dynamics from a set of short time dynamics simulations has been proposed.[29] There are many related techniques exploring similar idea, such as umbrella sampling[30–33] and

Milestoning.[34–39] BXD relies on the assumption that motion within the box is stochastic and that sequential collisions with box boundaries are uncorrelated. That is, the time between successive "collisions" with the box walls must be larger than the correlation time. To meet this requirement, the boxes must be longer than the correlation length, the length at which the trajectory loses memory of its state following the last collision. However, even in large boxes trajectories reflected by box boundaries can sometimes turn back rather quickly and so the procedure developed in ref [27] is used to remove any contribution from correlated velocity inversions to the number of hits h in the eq 1 for the rate coefficients and ensure BXD calculations are properly converged.

Providing the above conditions have been met, an estimate of the free energy profile along the reaction coordinate can be made from the uncorrelated box-to-box rate coefficients

$$K_{m-1,m} = \frac{k_{m-1,m}}{k_{m,m-1}} = \exp\left(-\frac{\Delta G_{m-1,m}}{k_b T}\right) \quad (5)$$

Thus, BXD is a powerful simulation technique as it allows kinetic, i.e. rate coefficients in the KME, and thermodynamic, i.e. Gibbs energy along a reaction coordinate or Potential of Mean Force (PMF), information to be found simultaneously, which reaches timescales long enough to simulate rare events. BXD results can be taken even further, for example differentiation along the reaction coordinate gives the force needed to unfold a molecule to a given position, which when applied to proteins can be used as an indication of mechanical stability.

The central advantage of BXD is that it can describe the behavior of atomistic systems on very long timescales, much greater than those accessible to straightforward molecular dynamics. BXD is a fully atomistic technique, but it can reach timescales of seconds and beyond. Although BXD assumes statistical equilibrium within each box, it can describe complicated nonequilibrium kinetics between the boxes. See for example ref [1] where BXD was used to explain complicated kinetics of peptide cyclization. This work uses the same

methodology as our previous paper [1] and below we will show how BXD kinetics can account for the dependence of unfolding force vs pulling velocity in the AFM pulling experiment.

2.2 Box-to-box rate coefficients and PMF from previous BXD simulations of protein pulling.

Previously we have determined the box-to-box rate coefficients along a reaction coordinate of distance between the two termini of titin's I27 domain, corresponding to its unfolding.[24,26,40] along end-to-end reaction coordinate.

After the initial structure of I27 had been equilibrated, simulations were conducted using the BXD subroutine implemented in CHARMM, with the EEF1 implicit solvent model and CHARMM 19 force field with a Langevin thermostat set to 303 K and a friction coefficient of 50 ps^{-1} to replicate bulk water.

To converge box-to-box rate constants BXD usually scans boxes back and force along the reaction coordinate several times. But once a large protein is fully extended along its end-to-end reaction coordinate it would not fold back to native state when BXD moves back towards the boxes with a smaller end-to-end distance. For that reason, in our previous work we extended proteins from their native state to full extension several times without folding the protein back. In all BXD trajectories the rate coefficients were similar, and their free energies (PMFs) have shown similar features.

Using the simulated rate coefficients and eq (5), a free energy profile along the reaction coordinate, chosen as the extension of the end-to-end distance from its native structure value, was generated. Figures 3a and b show the PMF vs end-to-end distance and its derivative

obtained from the BXD extension of I27 as calculated in the refs [24,40]. Point A corresponds to the native state of the protein, which would sit in the resulting PMF minimum, if I27 was also compressed as well as extended. The PMF at "negative extension" when protein is compressed is not shown as we are interested only in pulling of I27. With extension of the end-to-end distance the PMF increases rapidly at first with little change to the equilibrium structure of I27. This is a result of hydrogen bonding between β-sheets of I27. Initially, the force is shared between them, but once it becomes too great to withstand the hydrogen bonds break between the so-called A and G β-sheets of I27, which form the two ends of the protein amino-acid sequence. At point B they rupture quickly allowing the I27 domain to slacken and extend in length causing a reduction in force from the inflection point B to point C. Point D corresponds to the rupture of another set of hydrogen bonds between β-sheets formed in the middle of the amino-acid sequence. Further extension to approximately 250 Å would see the greatest increase in gradient as the protein approaches a fully extended linear conformation. When protein is "compressed" to the negative extensions, the PMF increases, but this region of PMF is not relevant to protein extension in pulling experiment.

The gradient of the PMF is shown at the frame (b), where characteristic points A-D can be seen much better than at the PMF itself. The maximal gradient, marked at the frame (b) by F_{max}, corresponds to the steepest region of the PMF curve, just before the β-sheet hydrogen bonds rupture. As described in the introduction above the unfolding force F_{unfld} reported in the experiment is not equal to $F_{max,}$ although there might be a correlation between the two. Below we will show how the unfolding force can be calculated with the help of BXD.

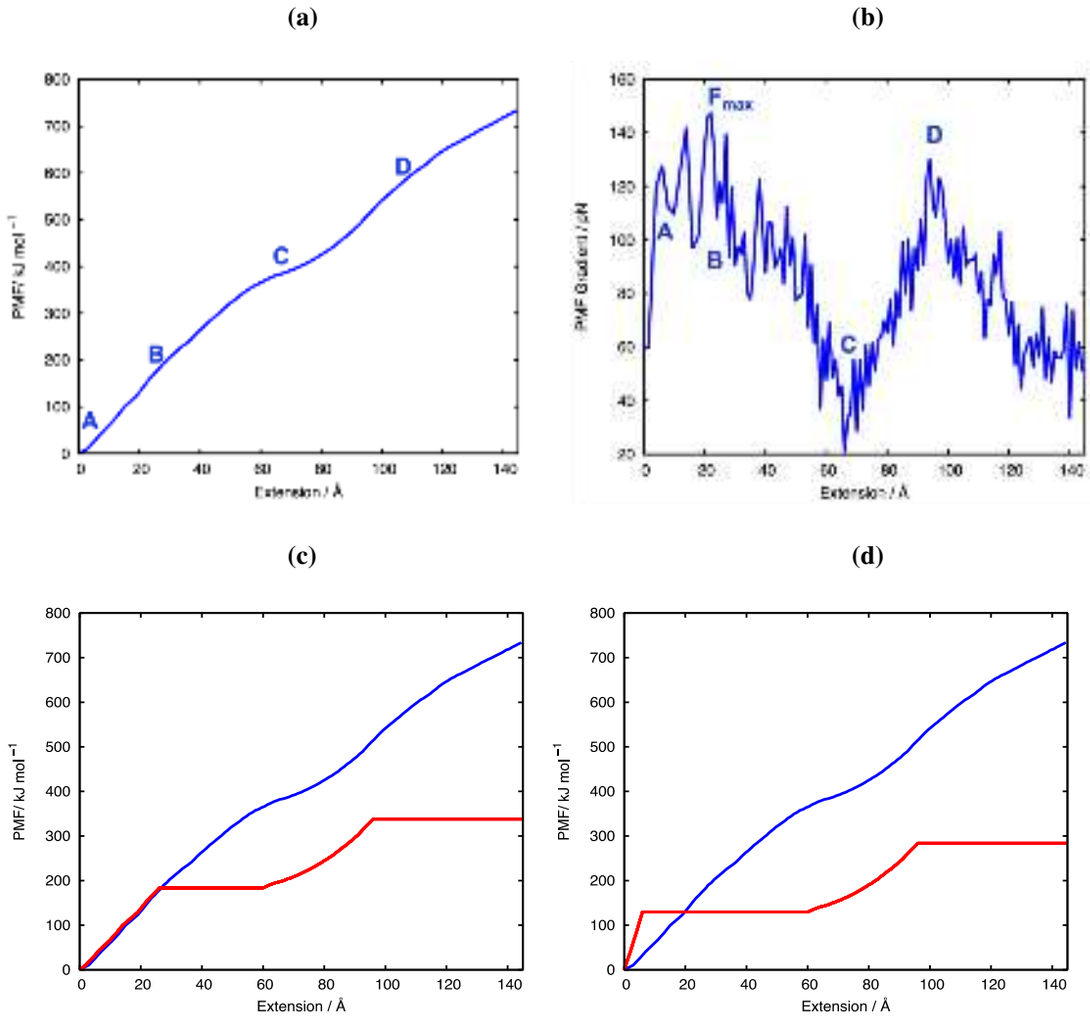

Figure 3. Frame a) shows PMF of I27, i.e. its free energy as a function of extension, calculated with BXD using implicit solvent model and b) its gradient representing low velocity pulling force. Point A corresponds to the native state of the protein and PMF minimum (not shown). Following this there is a steep increase in PMF to point B without any significant change in the equilibrium structure as the pulling force is spread over hydrogen bonds between I27's β-sheets. After reaching the point B the hydrogen bonds rupture almost simultaneously causing a drop in PMF gradient to point C as the protein slackens and extends. Further pulling increases the gradient up to point D as the next pair of β-sheets connected by hydrogen bonds comes under stress. The hydrogen bond link between these β-sheets is weaker, Fluctuation of the force reflects incomplete convergence of the calculation, which however capturers qualitatively the main features of the PMF. Frame c) shows a modified PMF1 with flat regions 25Å- 60Å and 95Å-145Å to account for the formation of hydrogen bonds with water and frame d) shows PMF2 with flat regions 5-60 Å and 95-145 Å as well as multiplication of the upwards rate coefficients before 5 Å by 0.0025. This modification provides the best fit to experiment.

In this paper we will use the results of the refs[24,40] to describe the unfolding kinetics in AFM experiment. We use previously obtained rate coefficients to develop a kinetic model of the

pulling process to model the experimentally observed dependence of unfolding force on pulling velocity.

To obtain a good description of the experiment we had to modify the PMF obtained in the ref[24]. Modified PMF1 and PMF2 are shown at the frames (c) and (d) of the Figure 3. The implicit solvent model used in the Refs[24,40] underestimates the effect of hydrogen bond formation between the newly ruptured protein beta sheets and the surrounding water molecules. Hydrogen bond formation significantly lowers the PMF of the system after point B in figure 3 (point of rupture) so that low gradient regions of the PMF curve should become even flatter. If, for extensions at which protein-solvent hydrogen bond formation is important, the rate coefficients corresponding to the original PMF in figure 3 (a) are replaced by their geometric average, the PMF becomes flat in these regions. Frame 3(c) shows the modified PMF, with flat regions introduced in the regions 25Å-60Å and 95Å-145Å, both around the inflection points B and D in figure 3(a). Frame 3(d) has flat regions at 5-60 Å and 95-145 Å along with multiplication of the BXD rate coefficients before 5 Å extension by 0.0025 so that the PMF value at the flat region is similar to that of point B in 3(a). As will be shown below this modification allows to achieve unfolding forces in better agreement with those from experiment.

2.3 Accounting for cantilever dynamics.

BXD assumes equilibrium within each box, allowing box-to-box rate constants to be defined. However, global equilibrium is not required, and as a result BXD is capable of describing nonequilibrium kinetics with the help of the Master Equation. In the case of protein unfolding assisted by AFM even if initially the protein was in equilibrium the motion of the cantilever distorts the initial equilibrium between boxes, and makes the population move from one box to the next.

Effective modification of the unbiased BXD rate coefficients and subsequent free energy to account for this can only be achieved if a term representing the interaction with the cantilever responsible for pulling the protein is included in the simulation. Similar to the refs[2,41], we assumed that the PMF of the system comprising of a protein molecule and a pulling cantilever is a sum of protein free energy of extension and mechanical potential energy of cantilever extension. Following many other approaches[15,23,42–44] we chose to model the cantilever as a harmonic spring with potential energy:

$$V_{harm} = \frac{kx^2}{2} = \frac{k[(r-r_0(t)])^2}{2} \quad (6)$$

where k is the cantilever spring constant and x is the displacement of the cantilever tip from its initial position, given by the box position along the reaction coordinate, r, minus the time dependent position of the tip $r_0(t)$.

The tip is moved with velocity v such that its position at time t is given by:

$$r_0(t) = r_0(0) + vt \quad (7)$$

where $r_0(0)$ is the initial position of the tip. The modified PMF becomes:

$$G_{tot}(r) = G_{BXD}(r) + V_{harm}(r,t) = G_{BXD}(r) + \frac{k(r-r_0(t))^2}{2} \quad (8)$$

The addition of this new time dependent potential, $V_{harm}(r,t)$ creates a new potential difference for diffusion of the population from one box into the next:

$$\Delta V_{harm_{m-1,m}} = V_{harm}(r_{m-1},t) - V_{harm}(r_m,t) \quad (9)$$

The box-to-box rate coefficients are modified to reflect the new potential difference between boxes imposed by the cantilever tip:

$$k_{m-1,m}(t) = k_{m-1,m}^{BXD}\, e^{-\frac{\Delta V_{harm_{m-1,m}}}{2RT}}$$
$$k_{m,m-1}(t) = k_{m,m-1}^{BXD}\, e^{\frac{\Delta V_{harm_{m-1,m}}}{2RT}} \quad (10)$$

Using the relationship between PMF and equilibrium constant *K*, the change in free energy for diffusion into box *m* from box *m*-1 can now be written as:

$$\Delta G_{m-1,m} = \Delta G_{tot_{m-1,m}} = -RT\ \ln(K)$$
$$= \Delta G_{BXD\ m-1,m} + \Delta V_{harm_{m-1,m}} \quad (11)$$

which is simply a rephrasing of the eq 8.

The modified time-dependent rate constants are calculated at time zero before any pulling takes place and used to generate the initial free energy. After that, an initial equilibrium population in all the boxes is assumed:

$$n_m(0) = \frac{e^{-\frac{G_m^{BXD}}{RT}}}{\sum_m e^{-\frac{G_m^{BXD}}{RT}}} \quad (12)$$

Each time step, Δt, in a simulation the position of the cantilever tip along the reaction coordinate, $r_0(t)$, moves to the point $r_0(t+\Delta t) = r_0(t) + v\Delta t$. New box-to-box rate coefficients are then generated and the KME (eqs 3 and 4) with initial conditions $n_m(\mathrm{t})$ is solved to calculate the corresponding box populations $n_m(\mathrm{t}+\Delta\mathrm{t})$ after time Δt, dragging the box populations along the reaction coordinate. Such a kinetic approach to AFM pulling has been outlined in the ref[2] albeit with only two states and model kinetic parameters. Here we implement this idea using many boxes with kinetic coefficients between them based on calculated by BXD atomistic simulations. Therefore, although in the end we are solving the KME, our BXD approach is based on fully atomistic simulations.

The box populations after each time step can be used to find the average peptide extension

$$\langle r(t)\rangle = \sum_m n_m(t) r_m \tag{13}$$

Then the experimentally observed force can be estimated according to the Hooke's law as

$$F_{exp}(r_0(t)) \;=\; -k(< r > -r_0(t)) \tag{14}$$

where $r_0(t)$ is the position of the cantilever at time *t*.

The blue line in figure 4 represents the sum of the harmonic spring and the flattened PMF profile. When the tip is moved to the right as in AFM pulling two minima appear. Protein rupture occurs upon transition of the populations from the first minimum to the second as shown by the gold arrow and can be described as before using the KME.

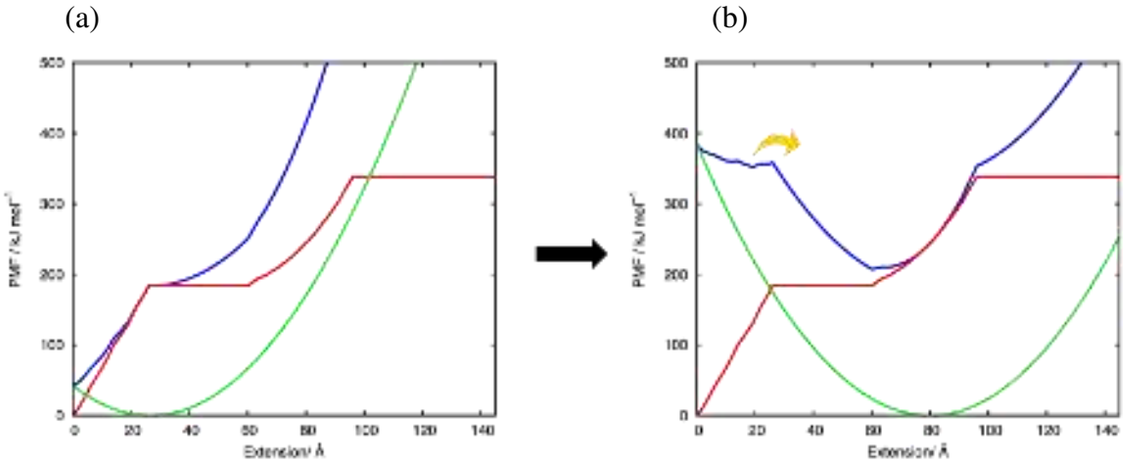

Figure 4: the Total PMF (blue) obtained by the addition of a harmonic spring (green) to the new flattened PMF1 profile (red) same as the red line at the Figure 3(c). Frames (a) and (b) are for two different positions of the cantilever, 25Å and 80Å respectively. Unfolding shown by the yellow arrow at the frame (b) occurs after the tip is pulled to the right and 2 minima appear in the total free energy. The figure covers 145 boxes as the box size of 1Å was used.

Using the kinetic approach described above the time evolution of populations along the total free energy of the system accounting for new hydrogen bonding can be seen as they are dragged along by the cantilever tip.

3. RESULTS

First, we performed a number of AFM pulling simulations for PMF1, using cantilever force constants in the range of k=1-10 pN/Å and pulling velocities covered in conventional and high-speed force spectrometry (HS-FS) experiments.[8,9,17] Figure 5 shows the dependence of the force (eq 14) on the cantilever position and time for two different pulling speeds, v=0.01 and v=10,000 μm/s shown in frames (a) and (b) respectively.

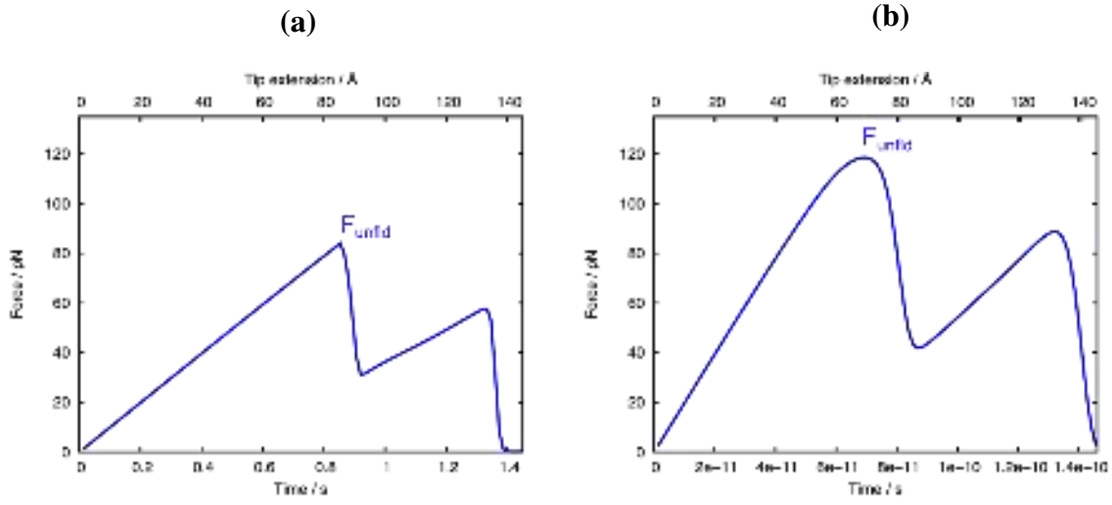

Figure 5 The dependence of the Hooke's force on time and cantilever position for v=0.01 (frame (a)) and v=10,000 μm/s (frame (b)) using a force constant k=2 pN/Å and a flattened PMF1 in the region of 25-60 Å and 95-145 Å. Pulling at higher velocities results in greater unfolding forces occurring on shorter timescales.

BXD reproduces the expected shape of the tooth for the range of velocities covered by HS-FS as well as showing an increase in force with speed. Importantly, figure 5 illustrates the power of BXD. The timescale of the protein pulling process shown at the left frame of the figure is in seconds, which is an extremely long for an atomistic simulation. Nevertheless, combining atomistic calculations of the box-to-box rate coefficients with the KME allows us to reach such timescales. Previously BXD was able to reach such long timescales in the refs[1,45].

Figure 6 illustrates the kinetics of unfolding. The lines shown by green, purple and cyan show the PMF1 (red line) with the addition of the harmonic potential energy for the cantilever

positioned at 40, 67 and 120 Å which it reaches at timesteps of 4 x10^7, 6.7x10^7 and 1.2x10^8 and 4 x10^2, 6.7x10^2 and 1.2x10^3 ns for cantilever speeds of 0.1 and 10000 μm/s respectively. First, although the total PMF is substantially distorted by the cantilever the population is still located near the original native state (green line). Then when the cantilever stretches another well at the total PMF is formed (purple line) and the population is transferred in there, which corresponds to the breaking of the first set of hydrogen bonds. Finally, when the cantilever is moved even further next well is formed and the unfolding continues, breaking the next set of hydrogen bonds (cyan). To illustrate how the force increases with pulling speed the frames (a) and (b) show the populations for two different pulling speeds, v=0.1 μm/s and v=10000 μm/s respectively. At higher pulling speeds, due to kinetic inertia the population lags behind which results in smaller average length of the protein $< r >$ and bigger force calculated with eq 14.

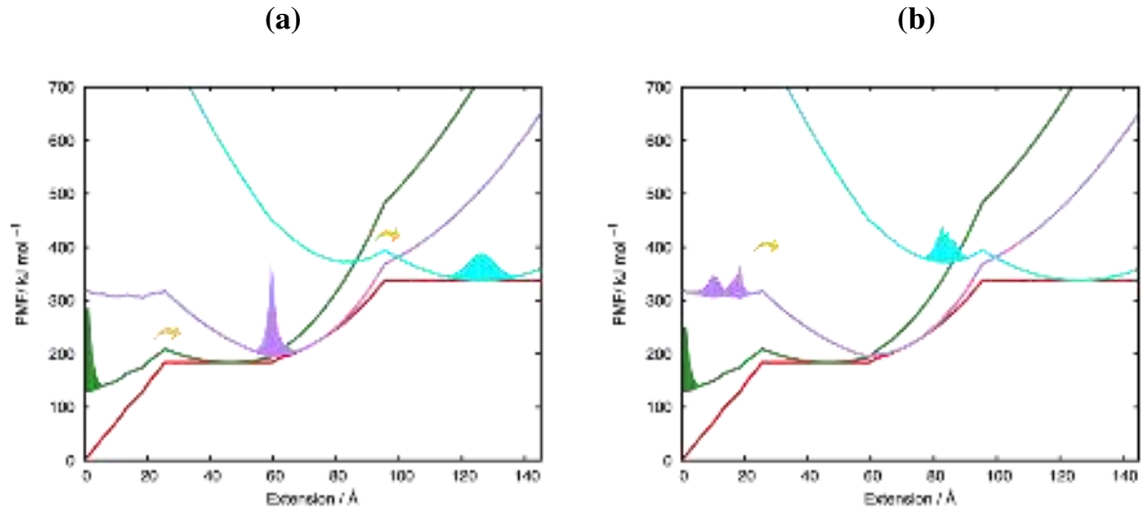

Figure 6 Population dynamics taken at three time points, corresponding to the cantilever extended by 40, 67 and 120 Å in an AFM pulling simulation using a force constant of k=2 pN/Å for low (fame a, v=0.1 μm/s) and high (fame b, v=10,000 μm/s) speeds. In the figure the leftmost well corresponds to a folded protein domain (green line) and a stretched cantilever and the right wells (purple and cyan) to unfolded protein domains and a relaxed cantilever. At higher pulling speeds there is less time to transition into the next well and so populations remain in the well for longer. The red line is the PMF1curve with flat regions at 25-60 Å and 95-145 Å, whilst the populations at an early, intermediate, and later timestep have been superimposed onto their corresponding modified PMF1+Vharm (eq 8) curve (shown in green, purple, and cyan).

At higher speeds a combination of kinetic inertia and less time available for transition into the next available well lead to an increased unfolding force.

With lower pulling velocities the kinetics drives the population along the unfolding coordinate and over the barrier [46] as soon as the unfolded state becomes thermodynamically lower or equal to the native folded state. Whereas pulling at higher velocities leaves less time for escaping to the second minima and the transition occurs with a delay. Therefore, the cantilever is shifted more to the right more resulting in a larger $r_0(t)$ and larger force (eq 14). Alternatively, this can be thought of as faster pulling reducing the time available to get over the barrier and so a lower barrier or greater force is required. Consequently, as pulling velocity is increased the population density fails to overcome the barrier and follows the cantilever with significant delay. Although such picture is known [2], BXD allows to visualize the dynamics in more detail.

Figure 7 shows the dependence of the peak force of unfolding, F_{unfld}, on the pulling speed. At low speeds F_{unfld} is independent of speed. Population transfer coinciding with protein rupture happens when the minimum of the right well reaches that of the left well. If the speed is low the cantilever does not move much during the time interval at which population transfer takes place. At higher speeds the cantilever can shift substantially during this time, resulting in additional Hooke's force and an increase in F_{unfld}. The force increases linearly with the logarithm of the pulling speed. Similar behavior has been yielded by the model approaches[2], but BXD yields this picture based on atomistic simulations.

Importantly, Figure 7 shows the dependence of F_{unfld} on pulling velocity for different force constants of the cantilever. For all force constants there is no such dependence for low v. This is because at low v the unfolding occurs after the next well becomes thermodynamically equal to the previous well and if the pulling is slow the cantilever does not move far during the unfolding. At higher velocities F_{unfld} shows a linear dependence on log(v) as in the previous work[2]. The dependence of the F_{unfld} on pulling speed shows a "kink" between flat region and the region of linear growth.

Also similar to the ref[2] BXD reveals a peak unfolding force dependent on the stiffness of the cantilever, with F_{unfld} increasing with increased cantilever stiffness. By moving the cantilever to the right creates a second minimum in the PES and transition into it defines entering the unbound state. Multiple bonds must break to unfold a protein. Any bonds in the protein that rupture from thermal fluctuations alone are held in place long enough by the rest of the structure to reform, and so an external force is required to destabilize all of the bonds for long enough for complete rupture. Depending on the cantilever force constant, the slope of the additional potential varies, which controls the steepness of the wall to 'climb' to reach the forming second minimum. Therefore, the minimum value of the external force depends on the cantilever stiffness.

This applies at very slow loading rates near where global equilibrium can be assumed. But at higher pulling speeds the unfolding force follows Bell's model in which the changing external force exponentially amplifies the unfolding rate, leading to non-equilibrium unfolding kinetics and a logarithmic force-pulling speed relationship. [2,13] At this point, kinetic parameters including the unfolding rate and the distance to the transition state begin to control the unfolding force and the cantilever stiffness becomes less relevant.

Reference [2] predicts that if a typical unfolding force versus the logarithm of pulling speed plot is produced for cantilevers of different stiffness over a large enough range of speeds, then there will be several flat lines for each force constant in the near equilibrium regime, followed by the linear increase in force associated with Bell's model at higher speeds. [2,13]

Figure 7 is an example of this; however the trend is seen for velocities higher than predicted. But as figure 8 shows, with the introduction of PMF2 (figure 3, frame (d)) this trend shifts towards the expected range of pulling velocities.

To the best of our knowledge the dependence of the force on the cantilever force constant has not been investigated experimentally in a systematic manner, but such experiment could

serve as a verification of the theory. Combined with BXD simulations such measurement could also serve as a source of information about the details of the PMF.

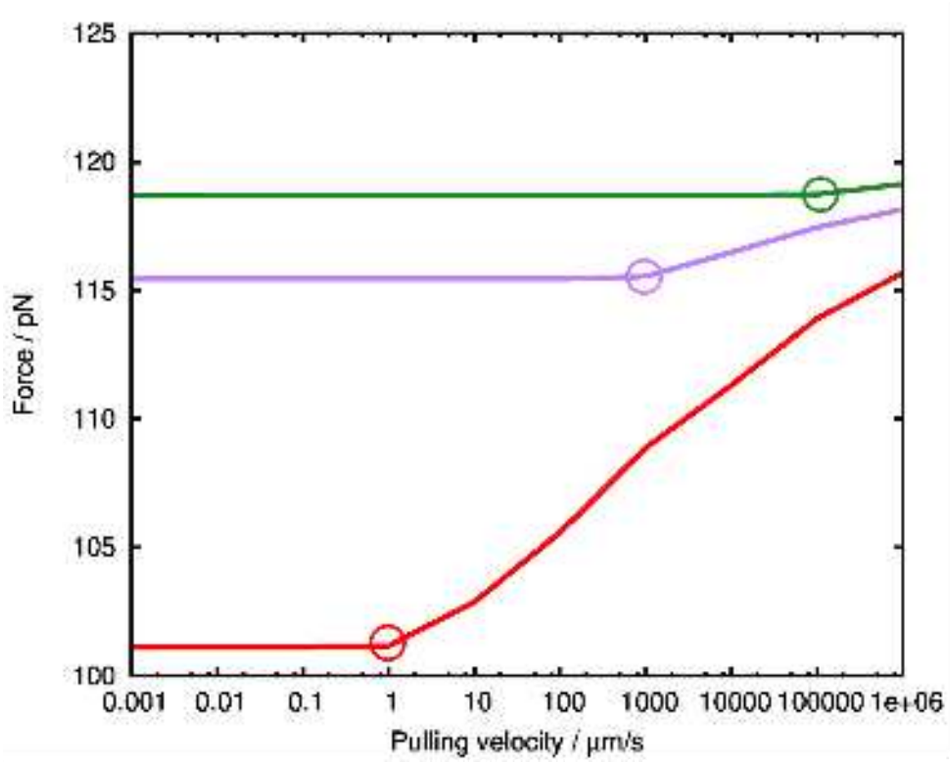

Figure 7 The dependence of the unfolding force on the pulling speed. At the lowest pulling speeds the force is independent of v. With increased pulling velocity populations have less time to escape the first well and cross the transition state to unfolding resulting in a higher unfolding force. Increasing the cantilever force constant increases the overall unfolding force and shifts the max force – pulling velocity curve to the right. All lines on the graph are for simulations done with a PMF flattened in the region of 25-60 and 95-200 Å as in figure 3(c), with the red line using a cantilever with 2 pN/Å, purple with 3 pN/Å and green k= 4 pN/Å. Circles mark each velocity at which the 'kink' in force spectrum appears as the force shifts from independent of speed, to linearly increasing with it,

Everywhere above we have used the PMF and rate coefficients calculated from previous BXD molecular dynamics simulations [24,40] with only some corrections to account for the interaction of protein with the solvent. BXD shows a dependence of F_{unfld} on pulling velocity. In the recent HS-FS experiment [8] the dependence of F_{unfld} on the pulling speed has been measured. Like all MD simulations BXD relies on a force field, which is not entirely accurate, and its variations can significantly alter the outcome of the calculations. Given these uncertainties as well as ones from converging errors and the impact they can have on BXD rate

coefficients, we have introduced additional changes to the BXD rate coefficients in order to fit the calculated force-pulling speed dependence to that of experiment.

PMF2 was introduced which is shown in figure 3 frame (d). In PMF2 the initial steep rise region was made shorter and steeper as shown in the figure.

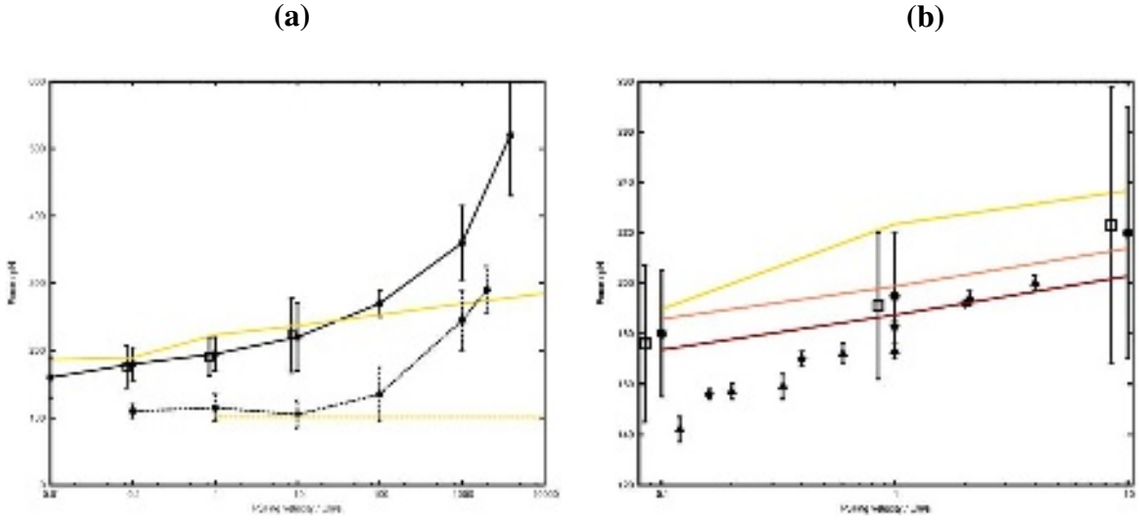

Figure 8. (a) Fit of BXD pulling calculations using a spring constant of 10 pN/Å and PMF2 to the experimental HS-FS data using different parameters. The black lines are taken from the dynamic force spectrums for I27 (solid line, square points from conventional AFM and circular from HS-FS) and its unfolding intermediate (dashed line) in ref [8]. The gold lines are for the flattened PMF in figure 3(d) and show the overall maximum unfolding force as a function of pulling speed (solid line) and our second maxima for each pulling seed, corresponding to the intermediate unfolding species in ref [8] **(b)** BXD calculations match experiment at conventional AFM speeds. The top gold, middle orange and bottom maroon lines are for simulations on PMF2 with k=10, 4 and 2 pN/Å respectively. Experimental data taken from ref [8] is shown by black circles and squares as in frame (a), whilst that taken from refs [12] and [17] are shown by black diamonds and triangles.

Figure 8(a) shows the Force-speed dependence for our overall maximum unfolding force, F_{unfld}, and the second maxima in figure 5 corresponding to an intermediate unfolding event. A cantilever force constant of 10 pN/Å was used, the same as in the experiment [8]. These calculated forces have been compared to the overall and intermediate unfolding forces of I27 reported in the experiment.[8] Agreement with experiment has been achieved at conventional pulling speeds (v=0.1-10 μm/s), but BXD could not reproduce additional increase of the force seen in the high-speed experiment. Frame (b) shows our $F_{unfld,}$ compared to those of refs.[8,12,17] in the range of velocities usually seen in AFM experiments. We used cantilever force constants

of 10, 4, and 2 pN/Å applied to PMF2 as shown by the gold orange and maroon lines, whilst the experimental data shown by black circles, squares, triangles and diamonds uses k=10 [8], 5 [17] and 4 [12] pN/Å respectively. Our simulations show slightly higher unfolding forces than experimentally determined ones but some deviation is to be expected. Also comparing experimental results from different experimental setups should be done with caution. For example, alternative methods of sample preparation between different experiments can lead to variation in the observed unfolding force. But qualitatively all the results in frame (b) are consistent. Both simulation and experiment show a linear relationship between unfolding force and velocity in this region and an overall increase in the force with cantilever spring constant is observed. This figure again highlights that an experiment to systematically investigate the dependence of the unfolding force on the cantilever force constant alone may be a useful in furthering our understanding of protein unfolding.

4. DISCUSSION AND CONCLUSIONS.

In this paper we demonstrate how BXD methodology can be used to simulate dynamics of AFM protein pulling at the slow cantilever speeds inaccessible for other atomistic simulations. The unbiased BXD simulations featured in refs [24,40] accelerate unfolding events in proteins by using the boxes as a ratchet to ease the transition over steep areas of the PES and do not contain any additional potential added to the system. Consequently, they can only be applied to AFM pulling at which the cantilever extension is slow enough for thermodynamic equilibrium to be maintained globally.[24] But, by subsequently modifying these rate constants to reflect the potential of the AFM tip, we can distort the kinetic equilibrium between the boxes, such that the populations move from box-to-box. In this way, we can model nonequilibrium kinetics occurring on a global scale though use of the KME whist still maintain the statistical equilibrium within each box assumed by BXD. Therefore, our simulations are capable of

modelling AFM pulling experiments over orders of magnitude covering the slowest velocities inaccessible to other simulation methods all the way up to those found in HS-FS. [8,9,15]

Protein dynamics on the timescale of seconds has been simulated. Using the results of unbiased BXD simulations as a starting point for our simulations has allowed us to obtain the sawtooth shaped force-extension profile symptomatic of CV AFM for all velocities in our simulations. This includes even the slowest pulling velocities for which the sawtooth appears on a timescale of tenths of seconds. Replicating the sawtooth at different pulling velocities is something previous atomistic simulations have failed to do and especially on such long timescales. In fact, for rare-event simulation it is the long timescales accessible to only BXD that have allowed such results to be obtained.

BXD yields the dependence of unfolding force vs pulling speed similar to those obtained previously.[2] At low pulling speeds the unfolding force is independent of the speed but at higher speeds it is followed by a Bell-Evans approximate linear increase with the logarithm of pulling speed. The difference, however, is that BXD uses kinetic parameters based on atomistic simulations, not simply phenomenological parameters. Also, BXD is not a two-state model but uses many boxes along the reaction coordinate instead.

Figure 8 demonstrates the agreement of BXD dependence of F_{unfld} on v at slow and moderate pulling velocities, typical for conventional AFM experiments, for two unfolding events observed. In the experiment [8] the main unfolding event was interpreted as the rupture of the hydrogen bonds between A and G β-sheets, and our calculations support this picture. The weaker unfolding event was interpreted as the rupture of the connection between A' and G β-sheets prior to the main A-G rupture event. In BXD calculations after the main event we observe the breaking of hydrogen bonds connecting other β-sheets in the protein, which is also consistent with the experiment.[8] In the AFM pulling experiments it is not easy to interpret smaller peaks and humps, similar to the peak 3' at the figure 1. They can appear due to the events occurring before the rupture of the main set of hydrogen bonds, like the rupture of A-G structure suggested in the ref [8], but also due to an event after the rupture of the strongest set of

hydrogen bonds as the "unzipping" of another weaker set of hydrogen bonds for example. BXD calculations suggest the latter. More than one secondary event was reported in experiments and their interpretation is still ambiguous.

Our results match well with experiment at intermediate pulling speeds in which a linear increase in unfolding force with velocity is expected. Figure 8 shows our simulations lie within experimental error limits for AFM done using conventional apparatus and HS-FS at speeds ≤ 100 μm/s (Figure 8a, square and circular points respectively) taken from the reference [8]. However, similar to the previous theory [41], we were unable to reproduce rapid increase of the unfolding force with the speed observed in the ref [8] at higher than v=100 μm/s. It might be at these speeds the BXD kinetic description of pulling fails because the molecular dynamics is faster that the rate of protein-environment equilibration within each box. In the ref [8] additional contribution to the pulling force due to Stokes friction force was also reported at high pulling speeds.

In our simulations we observed the rupture of two sets of hydrogen bonds. The first set required higher unfolding force, which was consistent with the observations.[8] However, obtaining quantitative agreement with the experiment required adjustment of the previously calculated box-to-box kinetic coefficients and PMF. This adjustment accounted for the formation of hydrogen bonds between water and freed hydrogen bond sites in the ruptured β-sheets. This effect is not taken into account by the implicit solvent model used in the calculations of BXD box-to-box rate coefficients. We also had to make the first set of hydrogen bonds stronger by adjusting the steepness of PMF in the region responsible for the rupture of the first pair of β sheets. Currently we are working on explicit water simulations trying to understand the importance of the solvent.

In summary this paper shows how BXD can provide a bridge between atomistic simulations and protein pulling experiments allowing to make quantitative connection between the experiment and atomistic protein structure.

ACKNOWLEDGEMENT

The authors acknowledge Emanuel Paci for his valuable feedback on the work as well as Lorna Dougan for her insights into the AFM experiments. S.M's studentship was kindly provided by the Dr Simon Waterworth PhD Scholarship fund whilst D.S's was funded by EPSRC grant EP/P021123/1. In the past J.B.'s studentship was provided by EPSRC grant EP/J0001481/1.

DATA

The data is available upon request

REFERENCES

[1] D. V Shalashilin, G.S. Beddard, E. Paci, and D.R. Glowacki, J. Chem. Phys. **137**, 165102 (2012).

[2] A. Noy and R.W. Friddle, Methods **60**, 142 (2013).

[3] A. Minajeva, M. Kulke, J.M. Fernandez, and W.A. Linke, Biophys. J. **80**, 1442 (2001).

[4] E. von Castelmur, M. Marino, D.I. Svergun, L. Kreplak, Z. Ucurum-Fotiadis, P. V. Konarev, A. Urzhumtsev, D. Labeit, S. Labeit, and O. Mayans, Proc. Natl. Acad. Sci. **105**, 1186 (2008).

[5] F. Rico, A. Rigato, L. Picas, and S. Scheuring, J. Nanobiotechnology **11 Suppl 1**, S3 (2013).

[6] W.A. Linke and A. Grützner, Pflügers Arch. - Eur. J. Physiol. **456**, 101 (2008).

[7] H. Li and J.M. Fernandez, J. Mol. Biol. **334**, 75 (2003).

[8] F. Rico, L. Gonzalez, I. Casuso, M. Puig-vidal, and S. Scheuring, Science (80-.). **342**, 741 (2013).

[9] M. Rief, M. Gautel, F. Oesterhelt, J.M. Fernandez, and H.E. Gaub, *Reversible Unfolding of Individual Titin Immunoglobulin Domains by AFM* (1997).

[10] Y. Taniguchi, A. Kobayashi, and M. Kawakami, Biophys. (Nagoya-Shi, Japan) **8**, 51 (2012).

[11] R.B. Best and J. Clarke, Chem. Commun. 183 (2002).

[12] K.M. Tych, M.L. Hughes, J. Bourke, Y. Taniguchi, M. Kawakami, D.J. Brockwell, and L. Dougan, Phys. Rev. E Stat. Nonlinear, Soft Matter Phys. **91**, 012710 (2015).

[13] G. Bell, Science (80-.). **200**, 618 (1978).

[14] E. Evans and K. Ritchie, Biophys. J. **72**, 1541 (1997).

[15] G. Hummer and A. Szabo, Biophys. J. **85**, 5 (2003).

[16] B. Heymann and H. Grubmüller, *Dynamic Force Spectroscopy of Molecular Adhesion Bonds* (2000).

[17] D.J. Brockwell, G.S. Beddard, J. Clarkson, R.C. Zinober, A.W. Blake, J. Trinick, P.D. Olmsted, D.A. Smith, and S.E. Radford, Biophys. J. **83**, 458 (2002).

[18] K.S. and D.H. M. Dembo, D. C. Torney, Proc. R. Soc. London. Ser. B, Biol. Sci. **234**, 55 (1998).

[19] P.E. Marszalek, H. Lu, H. Li, M. Carrion-Vazquez, A.F. Oberhauser, K. Schulten, and J.M. Fernandez, Nature **402**, 100 (1999).

[20] N. Crampton and D.J. Brockwell, Curr. Opin. Struct. Biol. **20**, 508 (2010).

[21] E. Paci and M. Karplus, Proc. Natl. Acad. Sci. U. S. A. **97**, 6521 (2000).

[22] E. Paci and M. Karplus, J. Mol. Biol. **288**, 441 (1999).

[23] H. Lu and K. Schulten, Proteins Struct. Funct. Genet. **35**, 453 (1999).

[24] J.J. Booth and D. V Shalashilin, J. Phys. Chem. B **120**, 700 (2016).

[25] D.R. Glowacki, E. Paci, and D. V Shalashilin, J. Phys. Chem. B **113**, 16603 (2009).

[26] D.R. Glowacki, J. Booth, S. Vazquez, E. Martinez-Nunez, A. Marks, J. Rodgers, and D. V Shalashilin, Philos. Trans. R. Soc. Lond. A. **372**, 20130384 (2014).

[27] D.R. Glowacki, E. Paci, and D. V Shalashilin, J. Chem. Theory Comput **7**, 1244 (2011).

[28] E. Martínez-Núñez and D. V Shalashilin, J. Chem. Theory Comput. **2**, 912 (2006).

[29] D. V Shalashilin and D.L. Thompson, *Intramolecular Dynamics Diffusion Theory: Nonstatistical Unimolecular Reaction Rates* (UTC, 1997).

[30] J. Kästner, Wiley Interdiscip. Rev. Comput. Mol. Sci. **1**, 932 (2011).

[31] G.M. Torrie and J.P. Valleau, J. Comput. Phys. **23**, 187 (1977).

[32] G.M. Torrie and J.P. Valleau, J. Chem. Phys. **66**, 1402 (1977).

[33] S. D, Frenkel. B, *Understanding Molecular Simulation*, 2nd ed. (Academic Press, London, UK, 2002).

[34] L. Maragliano, E. Vanden-Eijnden, and B. Roux, J. Chem. Theory Comput. **5**, 2589 (2009).

[35] R. Elber, Biophys. J. **92**, L85 (2007).

[36] A.M.A. West, R. Elber, and D. Shalloway, J. Chem. Phys. **126**, 145104 (2007).

[37] E. Vanden-Eijnden, M. Venturoli, G. Ciccotti, and R. Elber, J. Chem. Phys. **129**, 174102 (2008).

[38] K. Kuczera, G.S. Jas, and R. Elber, J. Phys. Chem. A **113**, 7461 (2009).

[39] A.K. Faradjian and R. Elber, J. Chem. Phys. **120**, 10880 (2004).

[40] J.J. Booth, *New Applications of Boxed Molecular Dynamics: Efficient Simulation of Rare Events* (2016).

[41] R.W. Friddle, A. Noy, J.J. De Yoreo, and J.J. De Yoreo, Proc. Natl. Acad. Sci. U. S. A. **109**, 13573 (2012).

[42] M. Gao, M. Wilmanns, and K. Schulten, *Steered Molecular Dynamics Studies of Titin I1 Domain Unfolding* (2002).

[43] M. Balsera, S. Stepaniants, S. Izrailev, Y. Oono, and K. Schulten, Biophys. J. **73**, 1281 (1997).

[44] H. Lu, B. Isralewitz, A. Krammer, V. Vogel, K. Schulten, L. Hui, B. Isralewitz, A. Krammer, V. Vogel, K. Schulten, H. Lu, B. Isralewitz, A. Krammer, V. Vogel, and K. Schulten, Biophys. J. **75**, 662 (1998).

[45] J.J. Nogueira, Y. Wang, F. Martín, M. Alcamí, D.R. Glowacki, D. V. Shalashilin, E. Paci, A. Fernández-Ramos, W.L. Hase, E. Martínez-Núñez, and S.A. Vázquez, J. Phys. Chem. C **118**, 10159 (2014).

[46] Yu-Shiu Lo, A. Ying-Jie Zhu, and J.. Thomas P. Beebe, Langmuir **17**, 3741 (2001).

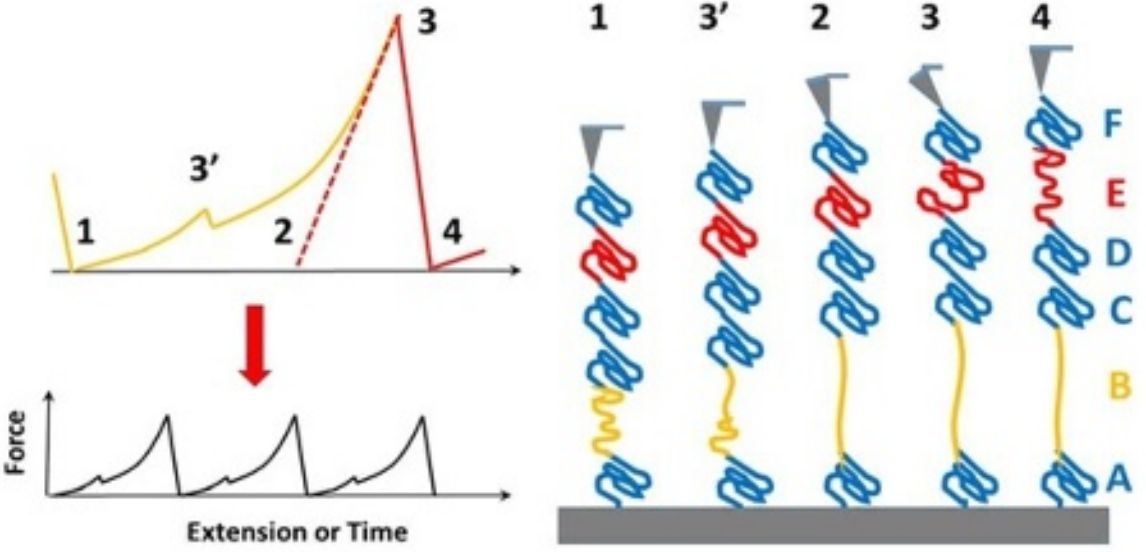
1
3'
2
3
4
Force
Extension or Time
1
3'
2
3
4
F
E
D
C
B
A

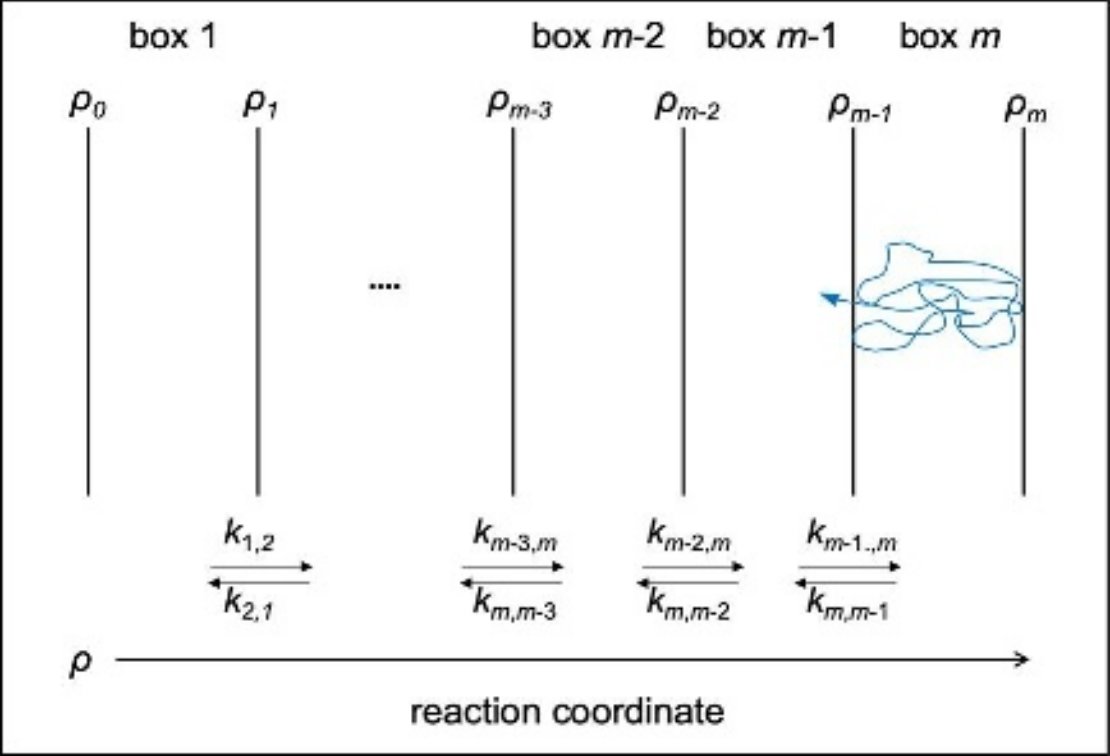
box 1
box m-2
box m-1
box m
ρ0
ρ1
ρm-3
ρm-2
ρm-1
ρm
....
k1,2
k2,1
km-3,m
km,m-3
km-2,m
km,m-2
km-1.,m
km,m-1
ρ
reaction coordinate

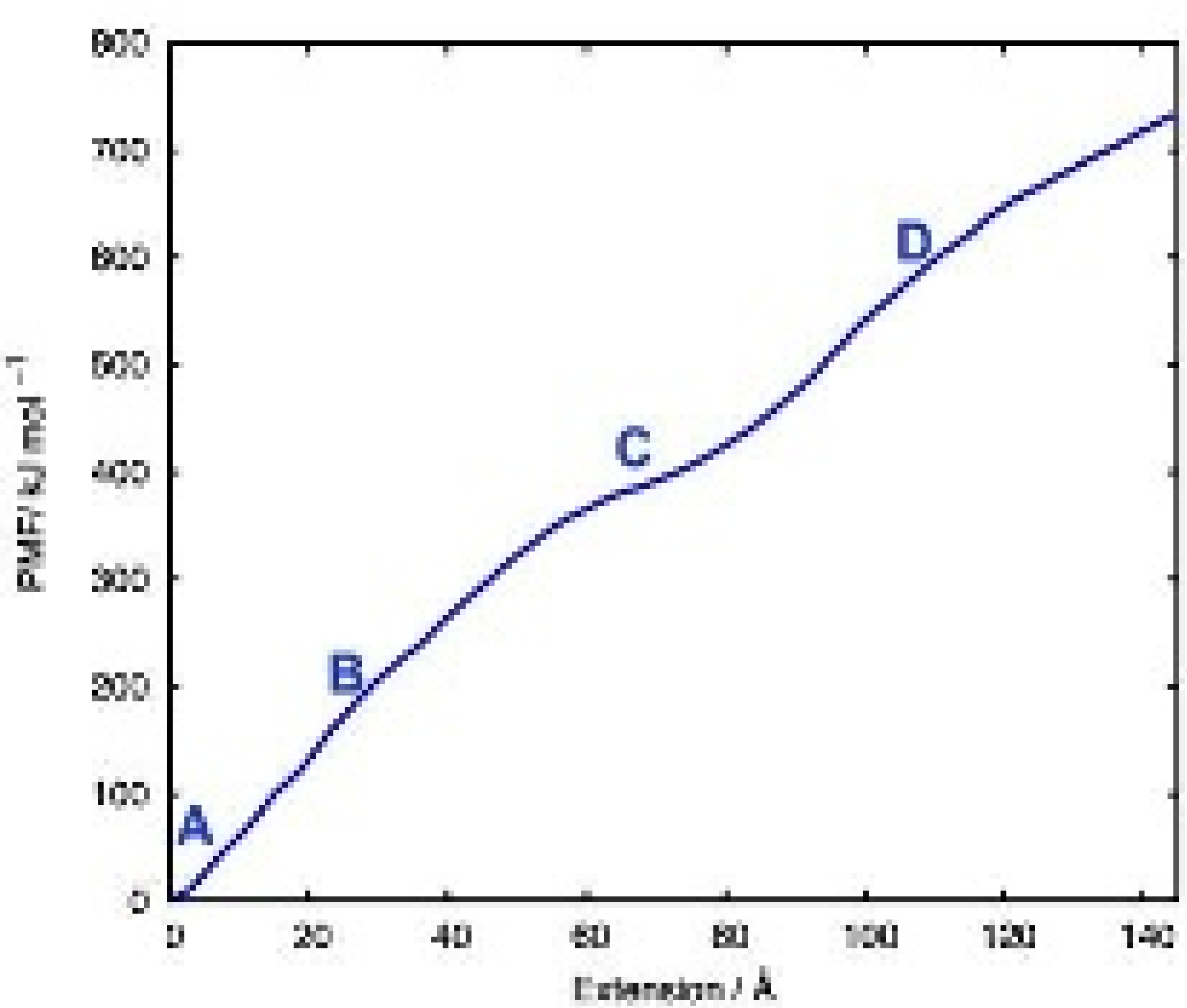
PMF/ kJ mol⁻¹
Extension / Å
A
B
C
D

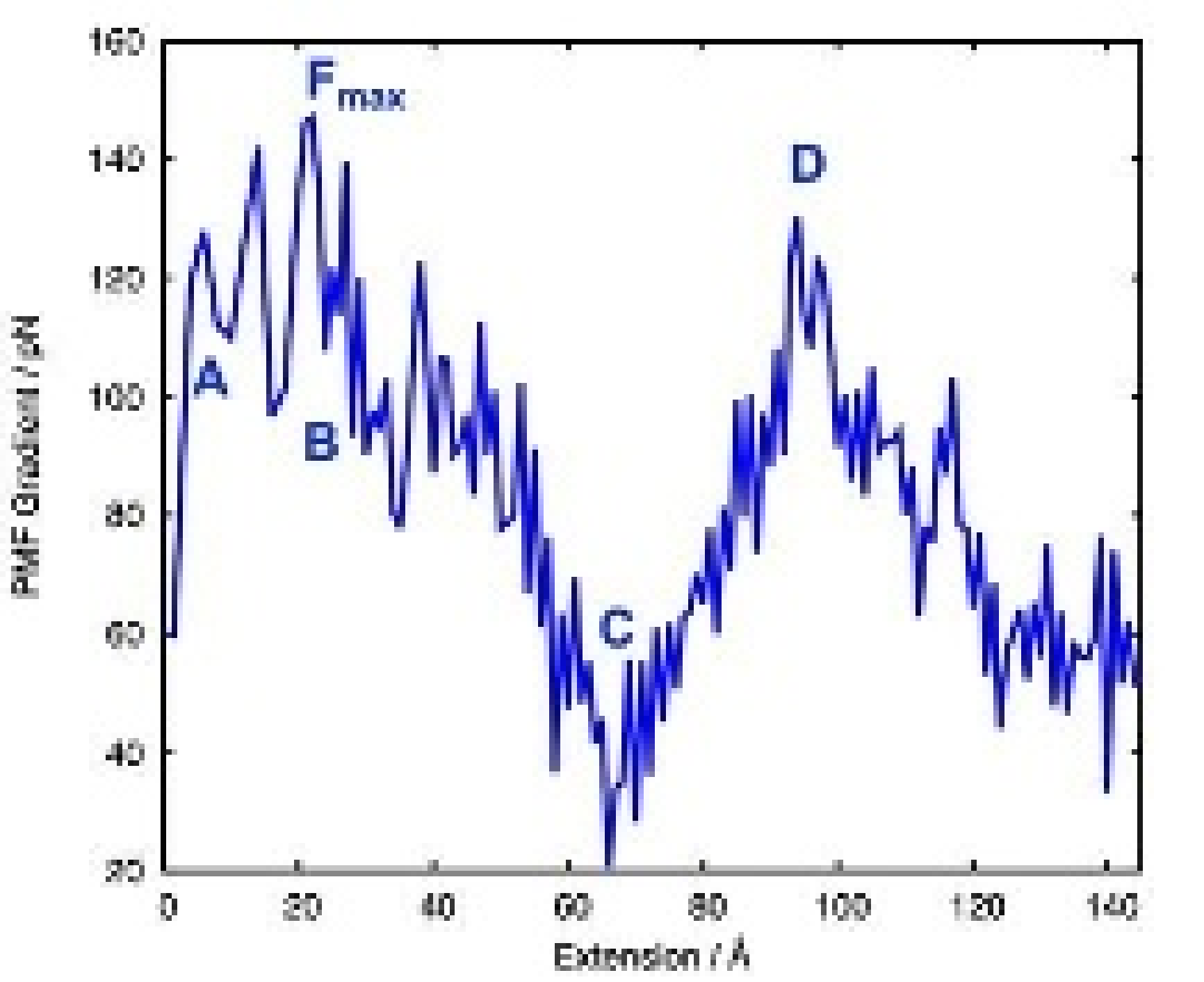
160
140
120
100
80
60
40
20
PMF Gradient / pN
0
20
40
60
80
100
120
140
Extension / Å
F_{max}
A
B
C
D

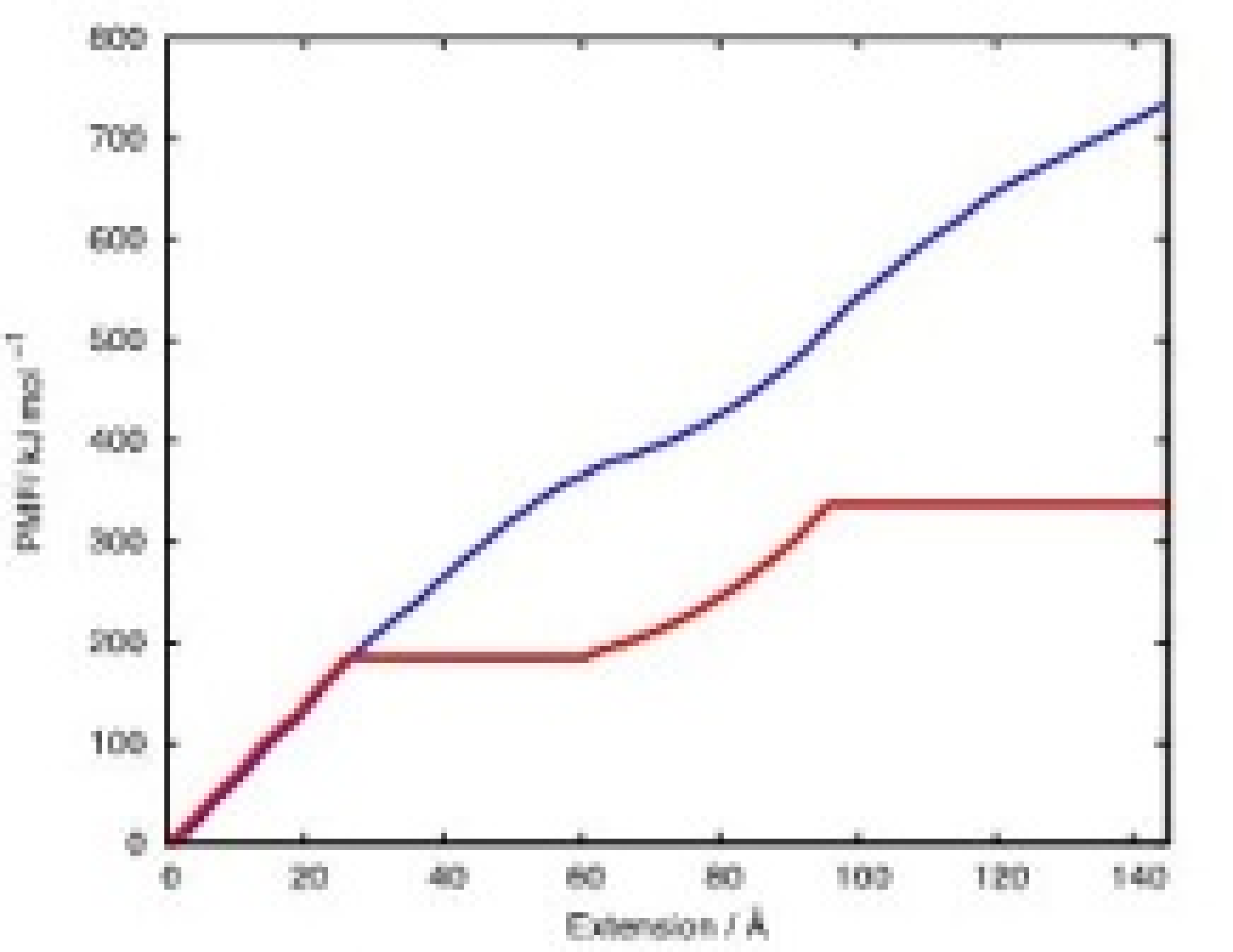
800
700
600
500
400
300
200
100
0
PMF / kJ mol^{-1}
0
20
40
60
80
100
120
140
Extension / Å

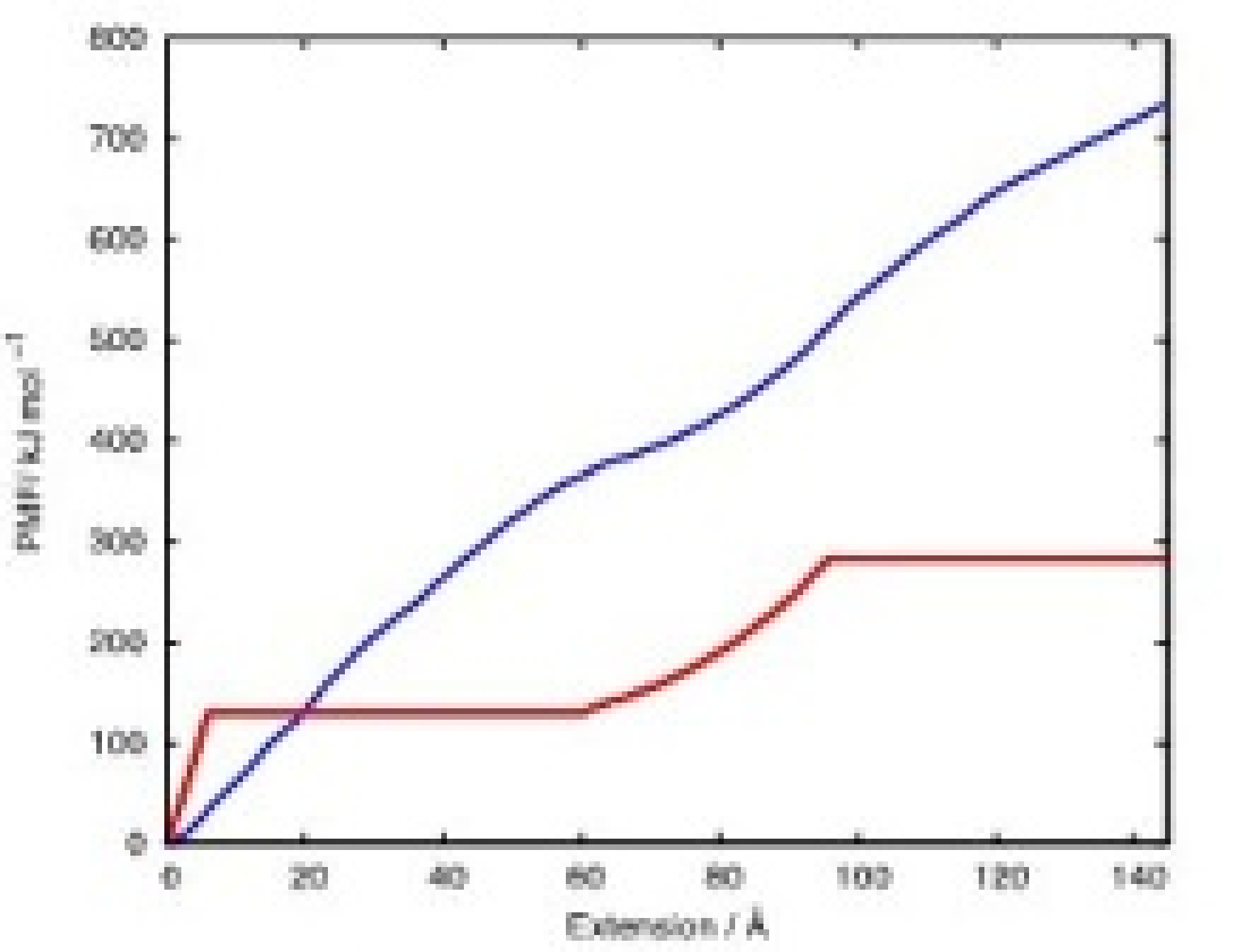
800
700
600
500
400
300
200
100
0
PMF / kJ mol^{-1}
0
20
40
60
80
100
120
140
Extension / Å

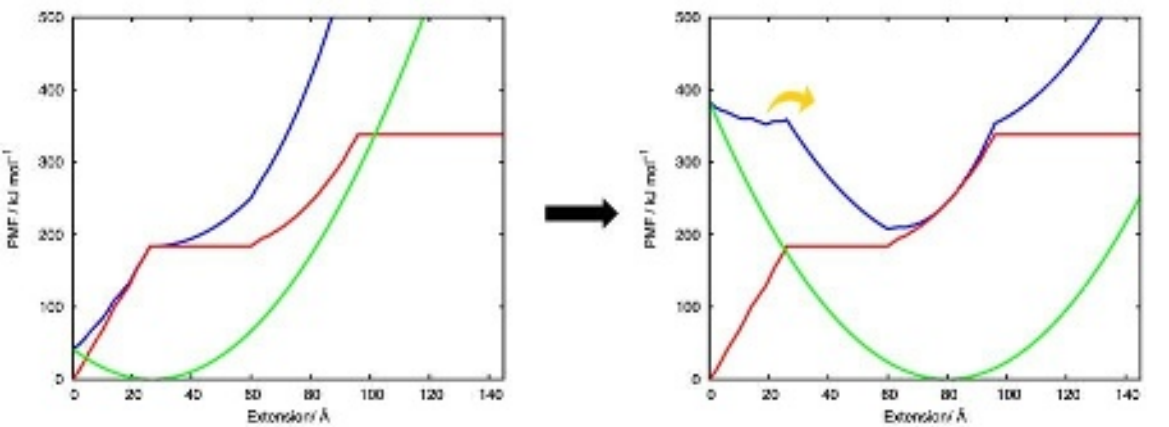
PMF / kJ mol⁻¹
Extension / Å
0
100
200
300
400
500
0
20
40
60
80
100
120
140

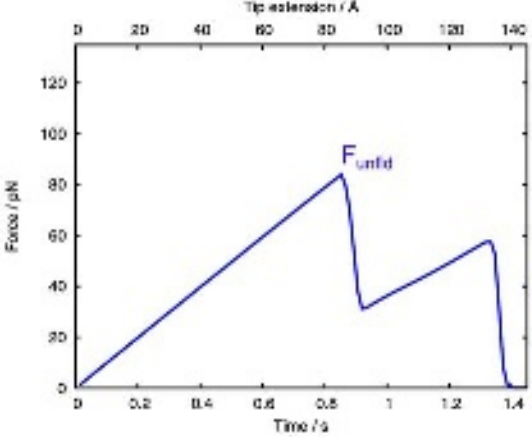
Tip extension / Å
0
20
40
60
80
100
120
140
Force / pN
0
20
40
60
80
100
120
Time / s
0
0.2
0.4
0.6
0.8
1
1.2
1.4
F_unfld

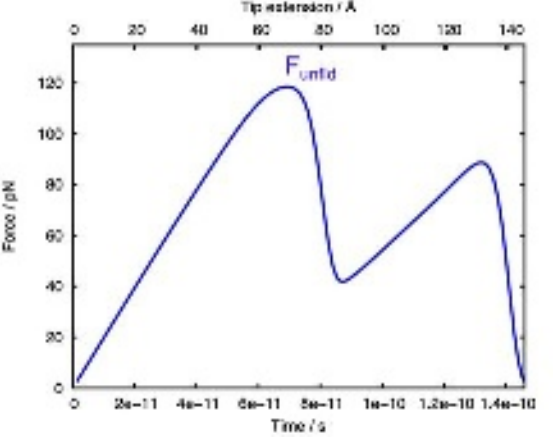
Tip extension / Å
0
20
40
60
80
100
120
140
Force / pN
0
20
40
60
80
100
120
Time / s
0
2e-11
4e-11
6e-11
8e-11
1e-10
1.2e-10
1.4e-10
F_unfld

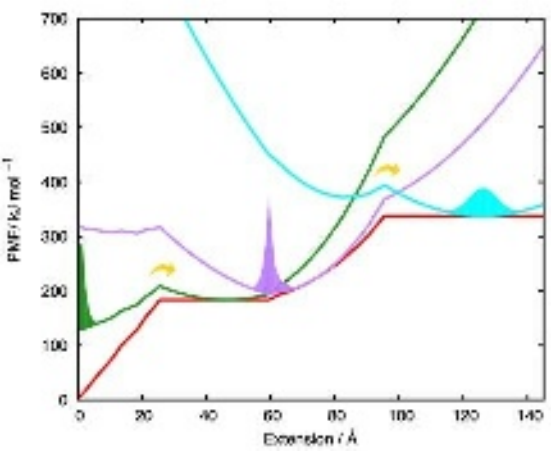
700
600
500
400
300
200
100
0
PMF / kJ mol^{-1}
0
20
40
60
80
100
120
140
Extension / Å

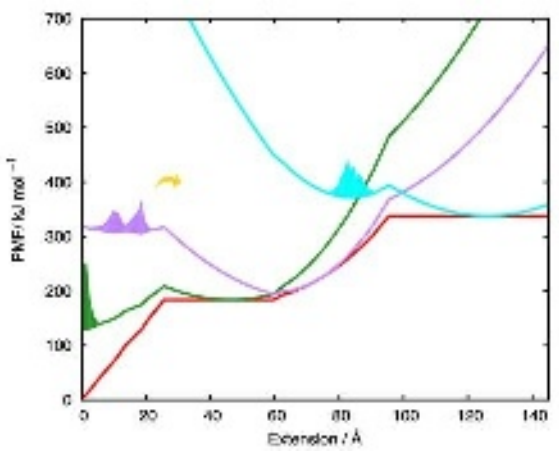
700
600
500
400
300
200
100
0
PMF / kJ mol^{-1}
0
20
40
60
80
100
120
140
Extension / Å

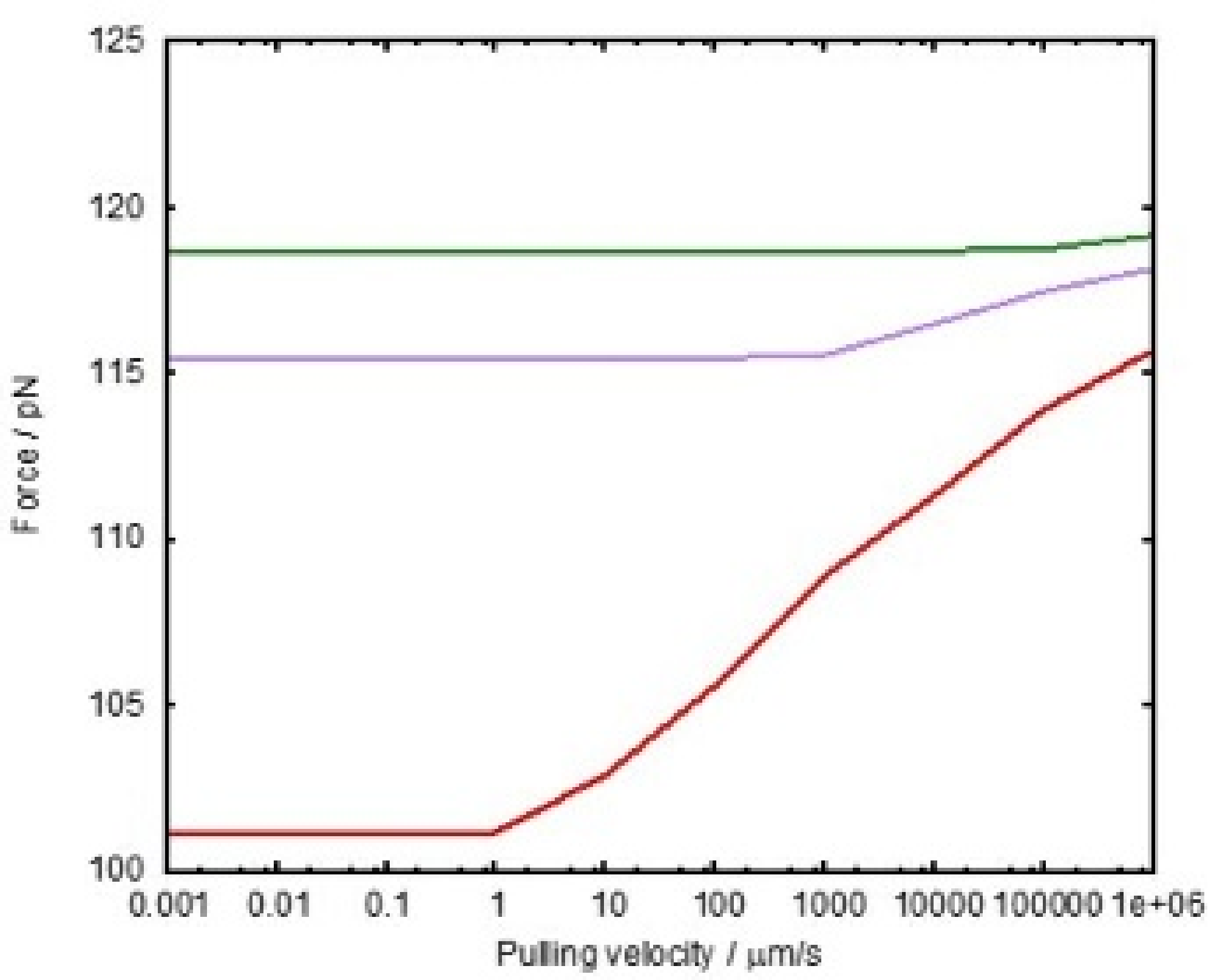
125
120
115
110
105
100
Force / pN
0.001
0.01
0.1
1
10
100
1000
10000
100000
1e+06
Pulling velocity / µm/s

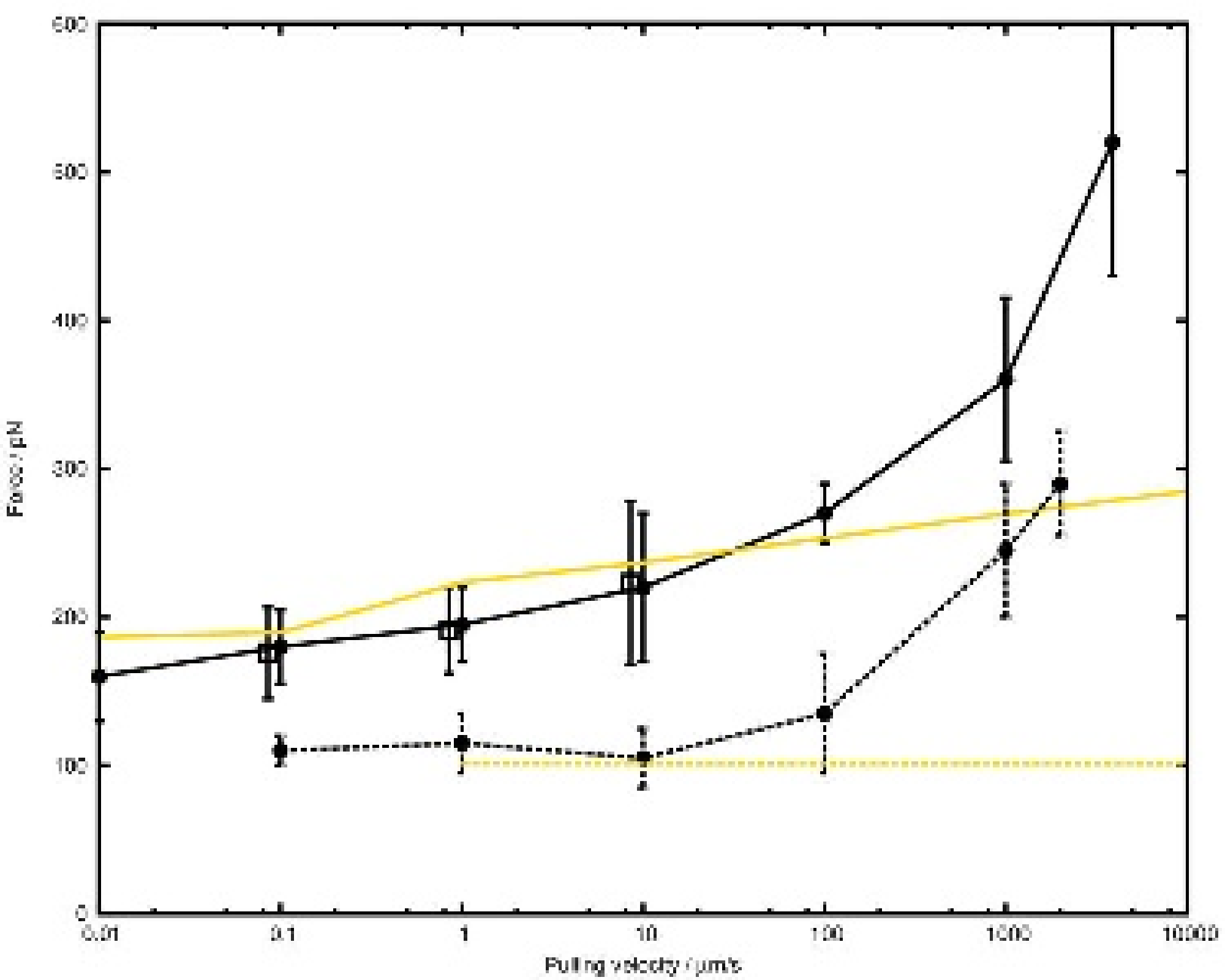
500
400
300
200
100
0
Force / pN
0.01
0.1
1
10
100
1000
10000
Pulling velocity / µm/s

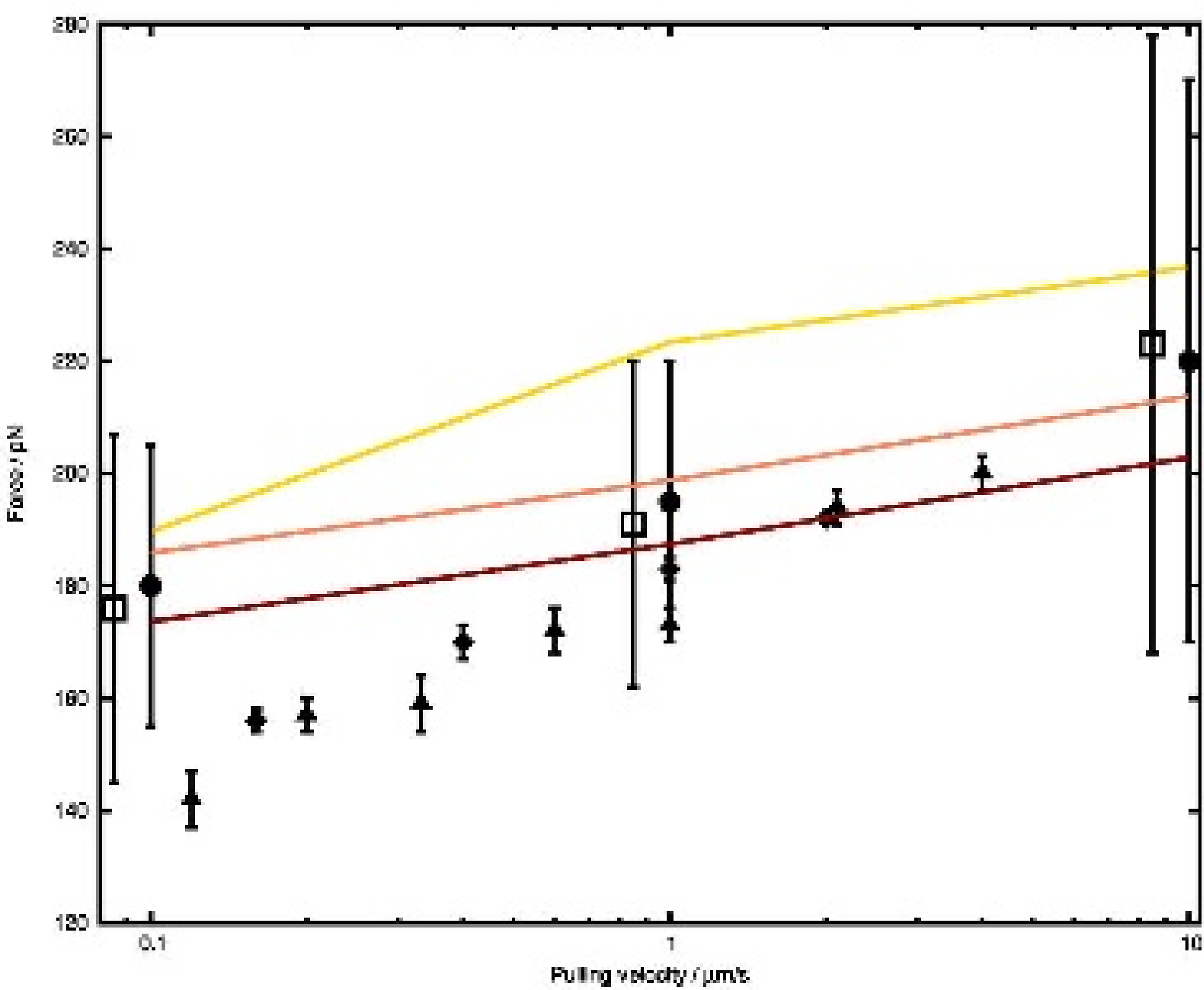
280
260
240
220
200
180
160
140
120
Force / pN
0.1
1
10
Pulling velocity / µm/s